2024 European Control Conference (ECC)
June 25-28, 2024. Stockholm, Sweden

Progressive Smoothing for Motion Planning in Real-Time NMPC

Rudolf Reiter[1], Katrin Baumgärtner[1], Rien Quirynen[2] and Moritz Diehl[1,3]

***Abstract*— Nonlinear model predictive control (NMPC) is a popular strategy for solving motion planning problems appearing in autonomous driving applications that include collision avoidance constraints. Non-smooth obstacle shapes, such as rectangles, introduce additional local minima in the underlying optimization problem. Using smooth over-approximations, e.g., ellipsoidal shapes, limits the performance due to their conservativeness. We propose to vary the smoothness and the related over-approximation by a homotopy. Instead of varying the smoothness in consecutive sequential quadratic programming iterations, we use formulations that decrease the smooth over-approximation from the end towards the beginning of the prediction horizon. Thus, the real-time iteration scheme applies to the proposed NMPC formulation, i.e., only one quadratic program needs to be solved at each time step. Different formulations are compared in simulation experiments and shown to successfully improve performance without increasing the computational burden.**

I. Introduction

Motion planning problems with obstacle avoidance are efficiently solved by derivative-based nonlinear optimization algorithms such as sequential quadratic programming (SQP) [1]–[6]. These algorithms pose limitations on the problem formulation to obtain beneficial numerical properties. Among others, a major desired property is smoothness in the constraints. Particularly for obstacles, which in autonomous driving (AD) applications are surrounding vehicles (SVs), it was shown that ellipsoids achieve superior performance compared to other formulations [7]. However, ellipsoids over-approximate the supposed rectangular SV shape by a large extent. Tighter formulations, such as higher-order norms can more accurately represent the shape, given an initial guess sufficiently close to an optimum [8], [9]. However, rectangular and higher-order ellipsoidal SV shapes are prone to introduce local minima and linearizations are discontinuous due to the obstacle corners. Thus, numerical solvers may get stuck in local minima, as shown empirically.

The presented idea builds on the assumption that predictions at the end of the horizon are more uncertain and planned motions can more easily be adapted. This flexibility makes the accurate SV shape less important which we exploit to represent the SV with more favorable numerical properties near the end of the horizon. The shape is transformed to a more non-smooth one towards the beginning of the horizon, cf., Fig. 1, where the uncertainty and flexibility are lower. Moreover, the receding horizon shifting of the previous solution provides a good warm start to a desirable local minimum. The loss of optimality due to constraint over-approximation can be reduced significantly if the over-approximations are rather tight near the beginning of the horizon. We refer to the proposed shape transformation as *progressive smoothing* with the particular constraint formulation *ScaledNorm*.

[1]Department of Microsystems Engineering, University Freiburg, 79110 Freiburg, Germany {rudolf.reiter, katrin.baumgaertner, moritz.diehl}@imtek.uni-freiburg.de
[2]Mitsubishi Electric Research Laboratories, Cambridge, MA, USA quirynen@merl.com
[3]Department of Mathematics, University Freiburg, 79110 Freiburg, Germany

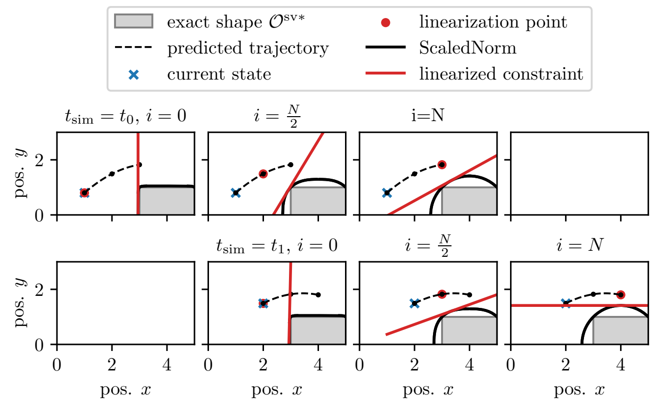

Fig. 1. Progressive smoothing with the proposed *ScaledNorm* of the obstacle shape along the prediction steps $i \in \{0, N/2, N\}$ for an NMPC prediction of N steps at simulation time $t_{\mathrm{sim}} = t_0$ (first row) and $t_{\mathrm{sim}} = t_1$ (second row). The *ScaledNorm* is smoothest for $i = N$ and tightest for $i = 0$. Each plot shows the linearization of the *ScaledNorm* at the corresponding prediction step.

The novel approach builds on nonlinear model predictive control (NMPC) in the Frenet coordinate frame [7], which is summarized in Sec. II. The *ScaledNorm* and two alternative formulations, referred to as *LogSumExp* and *Boltzmann*, are introduced and analyzed among their essential numerical properties for obstacle avoidance in Sec. III. Within closed-loop simulations, the performance is compared in Sec. IV, including the overtaking distance, the susceptibility for getting stuck in local minima and the computation time.

A. Related Work

An abundance of authors have successfully applied NMPC for AD with obstacle avoidance [2]–[6], [10], and an accurate representation of obstacle shapes is a major concern.

Due to favorable numerical properties, over-approximating ellipses are used in [11], [12]. The authors in [8], [9], [13] introduce higher order norms and [14] uses the infinity norm. However, as shown within this work, they are susceptible to getting stuck in local minima. Several covering circles [15], [16], a smooth infinity norm approximation [10] referred to as ReLU^2, or separating hyperplanes [12], [17] are used to more accurately capture the shape, however, as shown in [7], the performance is worse compared to ellipses on several test examples.

The authors in [8] use homotopies combined with SQP iteration to improve convergence by smoothing obstacle shapes. Progressive *smoothing* refers to the idea of progressively smoothing and expanding obstacle shapes along the horizon. Equally, this can be formulated as progressively *tightening* the feasible set along the horizon as it was introduced in [18], [19]. In [18], the authors reformulate constraints as costs on a part of the horizon for reduced computational complexity. Despite originating from a different idea, asymptotic stability for a general class was shown for tightening in [19].

B. Contributions

We contribute a novel formulation for progressive smoothing of obstacle shapes and a numerical analysis with respect to obstacle avoidance for NMPC. In addition, we introduce two alternative formulations for progressive smoothing. Their performance in closed-loop simulations is evaluated and highlighted against other state-of-the-art formulations.

C. Preliminaries

For index sets the notation $\mathbb{I}(n) = \{0, 1, \dots, n\}$ is used. Furthermore, $\mathbb{Z}^+$ refers to the strictly positive integer numbers. With the operator $[x]_i$, the i-th element of the vector $x \in \mathbb{R}^n$ is selected and the expression $\lfloor x \rfloor$ is used to denote the $\mathrm{floor}(\cdot)$ function, i.e., rounding down. The spatial derivative is x'.

II. Problem Setting

The problem of motion planning and control of an autonomous vehicle is considered. Particularly, a vehicle is controlled in a structured road environment that either involves driving along a certain reference lane or approximating time-optimal driving for racing applications [3], [20], [21] while avoiding SVs of a rectangular shape.

As shown in several works [2]–[5], [7], [22], using NMPC with a model formulation in the Frenet coordinate frame (FCF) yields state-of-the-art performance. Notably, the presented method is independent of the coordinate frame chosen for the model representation. However, the model representation is essential for the NMPC formulation. In the following, the basic concept of the FCF NMPC is defined.

The FCF transformation projects Cartesian position states $p^{\mathrm{veh}} \in \mathbb{R}^2$, together with a vehicle heading angle $\phi \in \mathbb{R}$ into a curvilinear coordinate system along a curve $\gamma(\sigma) : \mathbb{R}^+ \to \mathbb{R}^2$ that is parameterized by its arc length $\sigma \in \mathbb{R}^+$. The so-called Frenet coordinate system is described by the tangent unit vector $\mathcal{T}(\sigma) = \gamma'(\sigma)$ and the normal unit vector $\mathcal{N}(\sigma) = \mathcal{T}'(\sigma) \left\|\mathcal{T}'(\sigma)\right\|^{-1}$. The angle of the tangent vector $\mathcal{T}(s)$ is denoted by $\phi^{\gamma}(s)$. Cartesian states $x^{\mathrm{c}} = [p^{\mathrm{veh}\top},\ \phi]^\top$ can be replaced by the FCF states $x^{\mathrm{f}} = [s,\ n,\ \beta]^\top$, where the longitudinal state s is

$$s(t) = \arg\min_{\sigma} \left\|p^{\mathrm{veh}}(t) - \gamma(\sigma)\right\|_2,$$

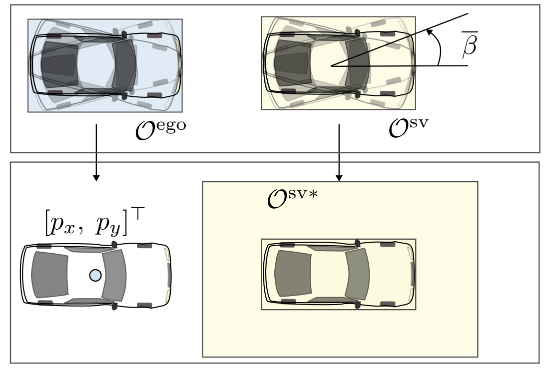

Fig. 2. Sketch of the considered SV in Frenet coordinates. The occupied spaces for the ego vehicle $\mathcal{O}^{\mathrm{ego}}$ and the SV $\mathcal{O}^{\mathrm{sv}}$ are approximated by rectangles that contains all road-aligned configurations with a maximum heading angle $\bar{\beta}$.

the lateral state is

$$n(t) = \Big(\gamma(s(t)) - p^{\mathrm{veh}}(t)\Big)^\top \mathcal{N}(s(t))$$

and the heading angle mismatch is $\beta(t) = \phi(t) - \phi^{\gamma}(s(t))$. Using the FCF states yields the state vector $x = [s,\ n,\ \beta,\ v,\ \delta]^\top$, including the steering angle δ and the velocity v. The inputs are $u^\top = [F^{\mathrm{d}},\ r]$ with the longitudinal acceleration force F^{d} and the steering rate r. According to [7], the dynamic equations of the FCF kinematic single-track model are

$$\dot{x} = f(x, u) = \begin{bmatrix} \frac{v\cos(\beta)}{1 - n\kappa(s)} \\ v\sin(\beta) \\ \frac{v}{l_{\mathrm{wb}}}\tan(\delta) - \frac{\kappa(s) v \cos(\beta)}{1 - n\kappa(s)} \\ \frac{1}{m}(F^{\mathrm{d}} - F^{\mathrm{res}}(v)) \\ r \end{bmatrix}, \tag{1}$$

where l_{wb} is the wheelbase and $\kappa(s) = \|\mathcal{T}'(s)\|$ is the curvature. The function $F^{\mathrm{res}}(v) = c_{\mathrm{air}} v^2 + c_{\mathrm{roll}} \mathrm{sign}(v)$ models the air and rolling friction with constants c_{air} and c_{roll}.

Taking the Minkowski sum of rectangular shapes for the ego and for an SV yields an inflated rectangular shape that allows to consider the ego vehicle as a point mass [23], cf. Fig. 2. We formulated collision avoidance as planning a trajectory outside of the rectangular shape in the FCF. Notably, rectangular shapes in the Cartesian coordinate frame can be integrated by techniques described in [7].

Pivotal to this work is the accurate representation of rectangular obstacle avoidance constraints. The over-approximated and inflated SV shape has the length l, the width w, summarized in $\theta = [l,\ w]^\top$ and the SV state is $z = [s^{\mathrm{sv}}\ , n^{\mathrm{sv}}\ , \beta^{\mathrm{sv}},\ v^{\mathrm{sv}},\ \delta^{\mathrm{sv}}]^\top$. With a scaling matrix

$$A(\theta) = \begin{bmatrix} \frac{2}{l} & 0 \\ 0 & \frac{2}{w} \end{bmatrix},$$

and the projection matrix $P_p \in \mathbb{R}^{2\times 5}$ that selects the position states, the SV shape can be normalized via the transformation

$\nu : \mathbb{R}^2 \to \mathbb{R}^2$, defined as

$$\nu(p; z, \theta) = A(\theta)(p - P_p z), \tag{2}$$

which is linear in p. With the normalized square denoted by

$$\mathcal{B} = \left\{\xi \in \mathbb{R}^2 \middle| \, \|\xi\|_\infty \leq 1\right\},$$

the obstacle can now be described as the following set

$$\mathcal{O}^{\text{sv}*}(z, \theta) = \left\{p \in \mathbb{R}^2 \middle| \nu(p; z, \theta) \in \mathcal{B}\right\}.$$

A superscript j is used to refer to a particular SV. Accordingly, the obstacle-free space concerning a single obstacle described by the state z^j and parameters θ^j can be written as

$$\mathcal{F}^{\text{sv}*}(z^j, \theta^j) = \left\{p \in \mathbb{R}^2 \middle| p \notin \mathcal{O}^{\text{sv}*}(z^j, \theta^j)\right\}. \tag{3}$$

Besides obstacle avoidance constraints, further constraints can be expressed for the states by the admissible set $\mathcal{X}$ and for the control inputs by the set $\mathcal{U}$.

In the following, the *nominal* NMPC formulation is introduced, which uses the exact obstacle formulation in the free set of (3). A nonlinear program (NLP) is formulated by direct multiple shooting [24] for a horizon of N steps. The model (1) is discretized with a step size t_d to obtain the discrete-time dynamics $x_{i+1} = F(x_i, u_i; t_\text{d})$. By setting a reference for states $\tilde{x}_i$ and controls $\tilde{u}_i = 0$ in the FCF with weights Q and R, and using a projection matrix $P_v \in \mathbb{R}^{1\times 5}$ that selects the velocity state, the NLP is

$$\min_{\substack{x_0,\ldots,x_N,\\ u_0,\ldots,u_{N-1}}} \quad \sum_{i=0}^{N-1} \|u_i\|_R^2 + \|x_i - \tilde{x}_i\|_Q^2 + \|x_N - \tilde{x}_N\|_{Q_N}^2 \tag{4a}$$

$$\begin{aligned}
\text{s.t.} \quad & x_0 = \hat{x}_0, && (4\text{b})\\
& x_{i+1} = F(x_i, u_i; t_\text{d}), i \in \mathbb{I}(N-1), && (4\text{c})\\
& u_i \in \mathcal{U}, \qquad i \in \mathbb{I}(N-1), && (4\text{d})\\
& x_i \in \mathcal{X}, \qquad i \in \mathbb{I}(N), && (4\text{e})\\
& P_v x_N = 0, && (4\text{f})\\
& P_p x_i \in \mathcal{F}^{\text{sv}*}(z_i^j, \theta_i^j), \, i \in \mathbb{I}(N),\\
& \qquad j \in \mathbb{I}(M-1). && (4\text{g})
\end{aligned}$$

The NLP (4) is linearized at the previous solution to obtain a parametric quadratic program (QP), which is solved within each iteration of the real-time iteration (RTI) scheme [1] after obtaining the state measurement $\hat{x}_0$. Note that the control admissible set also contains constraints for the lateral acceleration, cf. [7]. The ego vehicle is considered safe with zero velocity and no constraint violations. Hence, for simplicity, the equality constraint (4f) is used as a terminal safe set to obtain recursive feasibility.

III. Progressive Smoothing in Real-time NMPC

In the following our main contribution is introduced, an NMPC scheme that replaces the highly non-smooth constraint (4g) by a formulation that is successively smoothing the constraints along the prediction horizon.

The outstanding performance of the ellipsoidal constraint formulation [7] can be explained by favorable linearizations within SQP iterations that are often used to implement NMPC [25]. The ellipsoidal SV shapes are smooth and aligned with the road. Successive linearizations allow the shooting nodes to *traverse* around the smooth shape of the collision region. We use higher-order norms that are progressively smoothed along the prediction horizon and referred to as *ScaledNorm*. At the last prediction step N, the *ScaledNorm* is equal to the ellipsoid.

In the following, we use generalized coordinates $\xi \in \mathbb{R}^n$ for introducing the smooth over-approximations of the unit hypercube. For the considered vehicle motion planning problem, we have $n = 2$ and ξ is obtained via the linear transformation in (2), i.e. $\xi = \nu(p; z, \theta)$.

Formally, given two continuous functions $f(\xi) : \mathbb{R}^n \to \mathbb{R}$ and $g(\xi) : \mathbb{R}^n \to \mathbb{R}$, a homotopy map that depends on a homotopy parameter $\alpha \in [\underline{\alpha}, \overline{\alpha}]$, with $\overline{\alpha} \in \mathbb{R} \cup \{\infty\}$, is a continuous function $o(\xi, \alpha) : \mathbb{R}^n \times [\underline{\alpha}, \overline{\alpha}] \to \mathbb{R}$, with $o(\xi, \underline{\alpha}) = f(\xi)$ and $o(\xi, \overline{\alpha}) = g(\xi)$, for all $\xi \in \mathbb{R}^n$. The concept of a homotopy map is used in the following to transition from a smooth constraint $o(\xi, \underline{\alpha})$ to a tight constraint $o(\xi, \overline{\alpha})$.

Convexity of the SV shape in ξ is essential since it guarantees safe over-approximation within SQP iterates, cf. [7], [26]. The *tightening* property is crucial for recursive feasibility and is defined as follows.

Definition III.1. *A homotopy $o(\xi, \alpha) : \mathbb{R}^n \times [\underline{\alpha}, \overline{\alpha}] \to \mathbb{R}$ is monotonously* tightening *with an increasing α, if for all $\alpha_2 \geq \alpha_1$*

$$\{\xi \in \mathbb{R}^n | o(\xi, \alpha_2) \leq 1\} \subseteq \{\xi \in \mathbb{R}^n | o(\xi, \alpha_1) \leq 1\}.$$

The property of *over-approximation* is used to describe whether for any value of the homotopy parameter $\alpha \in [\underline{\alpha}, \overline{\alpha}]$, the smooth shape is over-approximating the rectangular shape $\mathcal{B}$.

Definition III.2. *A homotopy $o(\xi, \alpha) : \mathbb{R}^n \times [\underline{\alpha}, \overline{\alpha}] \to \mathbb{R}$ is an* over-approximation *of $\mathcal{B}$, if for $\alpha \in [\underline{\alpha}, \overline{\alpha}]$ it holds that*

$$\mathcal{B} \subseteq \{\xi \in \mathbb{R}^n | o(\xi, \alpha) \leq 1\}.$$

Definition III.3. *A homotopy $o(\xi, \alpha) : \mathbb{R}^n \times \mathbb{R}^+ \to \mathbb{R}$ is tight w.r.t. $\mathcal{B}$ if it is an over-approximation of $\mathcal{B}$ and*

$$\lim_{\alpha \to \overline{\alpha}} \{\xi \in \mathbb{R}^n | o(\xi, \alpha) \leq 1\} = \mathcal{B}.$$

A. ScaledNorm Formulation

The proposed *ScaledNorm* formulation is given via the homotopy $o^\text{p}(\xi; \alpha)$ defined as

$$o^\text{p}(\xi; \alpha) = \left(\frac{1}{n} \sum_{i=1}^{n} |\xi_i|^\alpha\right)^{\frac{1}{\alpha}},$$

with homotopy parameter $\alpha \in [2, \infty)$. Note that $o^\text{p}(\xi; \alpha)$ can be expressed as $o^\text{p}(\xi; \alpha) = \|n^{-\frac{1}{\alpha}} \xi\|_\alpha$ where $\|\cdot\|_p$ denotes the standard p-norm. For $\alpha = 2$, the set $\mathcal{O}^\text{p}(\alpha) = \{\xi \in \mathbb{R}^n | o^\text{p}(\xi, \alpha) \leq 1\}$ corresponds to a n-ball of radius $\sqrt{2}$. For $\alpha \to \infty$, we recover the unit square.

Property	*ScaledNorm*	*LogSumExp*	*Boltzmann*	*p-norm*	*ReLU²*	*cov. circles*
Progressive Smoothing	✓	✓	✓	✗	✗	✗
Convexity	✓	✓	✗	✓	✓	✓
Over-approximation	✓	✓	✓	✓	✓	✓
Homogeneity	✓	✗	✗	✓	✗	✓
Exact slack penalty	✓	✓	✓	✓	✗	✓

TABLE I

PROPERTIES OF THE CONSIDERED OBSTACLE FORMULATIONS.

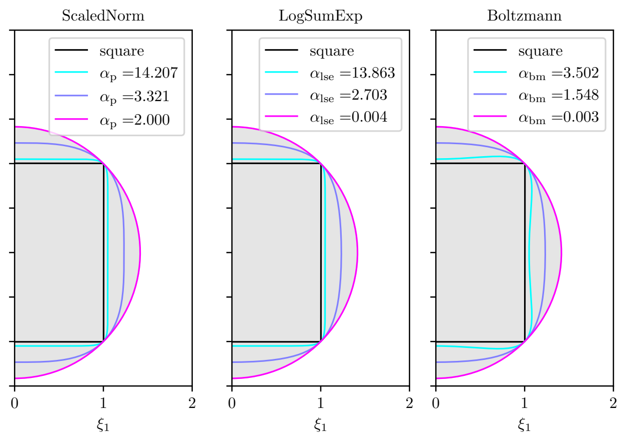

Fig. 3. Obstacle shape smoothing in normalized coordinates for the set $o(\xi, \alpha) = 1$. The associated tightening parameters $\alpha_{\{\cdot\}}$ are smoothed from a square shape (black) to a circle (magenta). The values of $\alpha_{\{\cdot\}}$ are chosen, such that the approximated widths and height are equal, measured at the axes. Notably, the non-convexity of the Boltzmann approximation can be seen for high values of α_{bm}.

The following lemma shows that the *ScaledNorm* formulation is monotonously tightening and over-approximating, as well as convex in ξ.

Lemma III.1. *The homotopy $o^{\mathrm{p}}(\xi;\alpha)$ with $\alpha \in [2,\infty)$ and defining the sets $\mathcal{O}^{\mathrm{p}}(\alpha) = \{\xi \in \mathbb{R}^n | o^{\mathrm{p}}(\xi,\alpha) \leq 1\}$ has the following properties:*

(i) *The function $o^{\mathrm{p}}(\xi;\alpha)$ is convex in ξ.*
(ii) *The sets $\mathcal{O}^{\mathrm{p}}(\alpha)$ are over-approximations of $\mathcal{B}$.*
(iii) *The sets $\mathcal{O}^{\mathrm{p}}(\alpha)$ are monotonously tightening in α.*

Proof. (i) Convexity in ξ follows directly from convexity of the α-norm for $\alpha \in [2,\infty)$.

(ii) Regard $\xi \in \mathbb{R}^n$ and let $\xi_{\max} = \max_i |\xi_i|$. We have

$$o^{\mathrm{p}}(\xi;\alpha) \leq \left(\frac{1}{n}\sum_{i=1}^{n} |\xi_{\max}|^{\alpha}\right)^{\frac{1}{\alpha}} = \xi_{\max},$$

which shows $o^{\mathrm{p}}(\xi;\alpha) \leq \|\xi\|_\infty$ and thus $\mathcal{B} \subseteq \mathcal{O}^{\mathrm{p}}(\alpha)$.

(iii) Let $\alpha_1 \leq \alpha_2$. With $\|\xi\|_{\alpha_1} \leq n^{\frac{1}{\alpha_1}-\frac{1}{\alpha_2}} \|\xi\|_{\alpha_2}$, we obtain

$$o^{\mathrm{p}}(\xi;\alpha_1) = n^{-\frac{1}{\alpha_1}} \|\xi\|_{\alpha_1} \leq n^{-\frac{1}{\alpha_2}} \|\xi\|_{\alpha_2} = o^{\mathrm{p}}(\xi;\alpha_2).$$

□

B. Alternative Formulations

We compare the proposed progressively smoothing *ScaledNorm* formulation to five alternative constraint formulations: (a) a higher order norm formulation [9] that is constant along the prediction horizon; (b) the ReLU^2 formulation as introduced in [10]; (c) three covering circles [15]; (d) a progressively smoothing *LogSumExp* formulation; (e) a progressively smoothing *Boltzmann* formulation. Their properties are summarized in Tab. I.

A visual comparison of the three progressively smoothing formulations – the *ScaledNorm* formulation, the *LogSumExp* formulation, and the *Boltzmann* formulation – is given in Fig. 3.

The *LogSumExp* formulation is defined via

$$o^{\mathrm{lse}}(\xi;\alpha) = \eta_{\mathrm{lse}}(\alpha) \log \frac{1}{2n} \sum_{i=1}^{n} \exp(\alpha\xi_i) + \exp(-\alpha\xi_i),$$

with homotopy parameter $\alpha \in (0,\infty)$ and normalization constant $\eta_{\mathrm{lse}}(\alpha)$ given as

$$\eta_{\mathrm{lse}}(\alpha) = \frac{1}{\log(\frac{1}{2}(\exp(\alpha)+\exp(-\alpha)))}.$$

The corresponding sets $\mathcal{O}^{\mathrm{lse}}(\alpha) = \{\xi \in \mathbb{R}^2 | o^{\mathrm{lse}}(\xi,\alpha) \leq 1\}$ over-approximate the unit square. For $\alpha \to 0$, we obtain $\mathcal{O}^{\mathrm{p}}(2)$; and for $\alpha \to \infty$, we recover the unit square as illustrated in Fig. 3. Furthermore, convexity of the *LogSumExp* function implies convexity of the sets $\mathcal{O}^{\mathrm{lse}}(\alpha)$.

The *Boltzmann* formulation, which is based on the Boltzmann (also *soft-max*) operator, is given as

$$o^{\mathrm{bm}}(\xi;\alpha) = \eta_{\mathrm{bm}}(\alpha) \frac{\sum_{i=1}^{n} \xi_i \exp(\alpha\xi_i) - \xi_i \exp(-\alpha\xi_i)}{\sum_{i=1}^{n} \exp(\alpha\xi_i) + \exp(-\alpha\xi_i)},$$

with homotopy parameter $\alpha \in (0,\infty)$ and normalization constant $\eta_{\mathrm{bm}}(\alpha)$ defined as

$$\eta_{\mathrm{bm}}(\alpha) = \frac{\exp(\alpha)+\exp(-\alpha)}{\exp(\alpha)-\exp(-\alpha)}.$$

As illustrated in Fig. 3, the sets $\mathcal{O}^{\mathrm{bm}}(\alpha_{\mathrm{bm}}) = \{\xi \in \mathbb{R}^n | o^{\mathrm{bm}}(\xi,\alpha_{\mathrm{bm}}) \leq 1\}$ over-approximate the unit square. For $\alpha \to 0$, we recover the set $\mathcal{O}^{\mathrm{p}}(2)$; and for $\alpha \to \infty$, we obtain the unit square $\mathcal{B}$. However, the *Boltzmann* function is nonconvex as illustrated by its nonconvex sublevel sets shown in Fig. 3.

C. Constraint Linearization and Homogeneity

During SQP or RTI iterations, the constraint function is linearized at the current iterate, here denoted by $\tilde{\xi}$, to derive the QP sub-problem. The following lemma shows that the linearization of the constraint is exact in the direction of the linearization point, i.e. the separating hyperplane obtained by linearizing the constraint is tight if the *ScaledNorm* formulation is used.

Lemma III.2. *Let $o^{p}_{\mathrm{lin}}(\xi;\tilde{\xi},\alpha)$ denote the linearization of $o^{p}(\xi;\alpha)$ at a linearization point $\tilde{\xi} \neq 0$. It holds that*

$$o^{p}_{\mathrm{lin}}(\gamma\tilde{\xi};\tilde{\xi},\alpha) = o^{p}(\gamma\tilde{\xi};\alpha)$$

for all $\gamma \in [0,1]$.

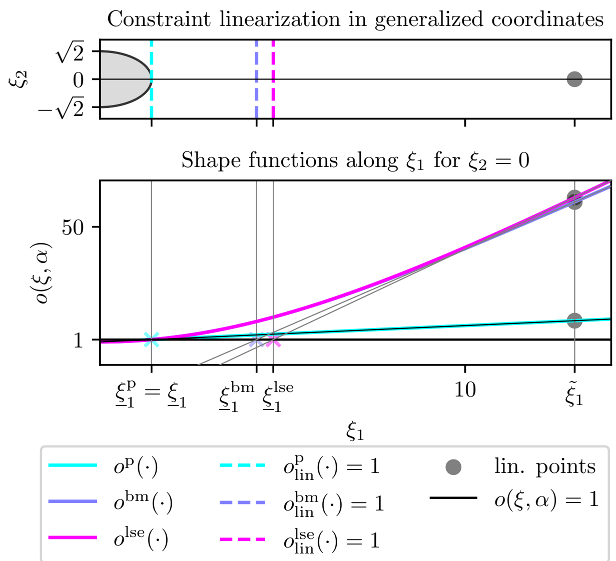

Fig. 4. Linearized constraints $o^{\{\cdot\}}_{\mathrm{lin}}(\cdot) \geq 1 \Leftrightarrow \xi \geq \underline{\xi}^{\{\cdot\}}$ for the generalized coordinates ξ at an linearization point $\tilde{\xi} = [\tilde{\xi}_1, 0]^\top$ for the smoothest approximation, i.e., $\alpha_{\mathrm{p}} = 2$ and $\alpha_{\mathrm{lse}} = \alpha_{\mathrm{bm}} \approx 0$. Related separating hyperplanes, i.e., $o^{\{\cdot\}}_{\mathrm{lin}}(\cdot) = 1$ are shown in the upper plot and the linearizations of the obstacle shape functions $o^{\{\cdot\}}(\cdot)$ along ξ_1 for $\xi_2 = 0$ are shown in the lower plot. Any p-norm is homogeneous, thus also for the *ScaledNorm* formulation it is true that $\underline{\xi} = \underline{\xi}^{\mathrm{p}}$ for any linearization point $\tilde{\xi}$.

Proof. The partial derivative of $o^p(\xi;\alpha)$ is given as

$$\frac{\partial o^p}{\partial \xi_i}(\xi;\alpha) = \frac{1}{n^{\frac{1}{\alpha}}}\left(\frac{|\xi_i|}{\|\xi\|_p}\right)^{p-1} \mathrm{sign}(\xi_i),$$

from which we conclude that $\nabla_\xi o^p(\xi;\alpha) = \nabla_\xi o^p(\gamma\xi;\alpha)$ for any $\gamma \in [0,1]$. For $\xi = \gamma\tilde{\xi}$, we thus obtain

$$\begin{aligned} o^p(\xi;\alpha) &= o^p(\tilde{\xi};\alpha) + \int_0^1 \nabla_\xi o^p(\tilde{\xi} + \tau(\xi - \tilde{\xi});\alpha)(\xi - \tilde{\xi})\,\mathrm{d}\tau \\ &= o^p(\tilde{\xi};\alpha) + \nabla_\xi o^p_{\mathrm{lin}}(\tilde{\xi};\tilde{\xi},\alpha)^\top(\xi - \tilde{\xi}) \\ &= o^p_{\mathrm{lin}}(\xi;\tilde{\xi},\alpha). \end{aligned}$$

□

This property, which is due to the homogeneity of the norm, is not shared by the *Boltzmann* and *LogSumExp* formulation as illustrated in Fig. 4.

D. NMPC Formulation using Progressive Smoothing

For each of the tightening formulations, a scheduling function $\alpha_i^{\{\mathrm{p,lse,bm}\}}$ is used that parameterizes the tightening parameter α according to the prediction time. Consequently, for each SV j and prediction step i, the free set is

$$\begin{aligned} &\mathcal{F}_i^{\{\mathrm{p,lse,bm}\}}(z^j,\theta^j) = \\ &\quad \left\{p \in \mathbb{R}^2 \middle| o^{\{\mathrm{p,lse,bm}\}}(p;\alpha_i^{\{\mathrm{p,lse,bm}\}}, z^j,\theta^j) \geq 1\right\}, \end{aligned} \tag{5}$$

and replaces the exact but non-smooth SV constraint in (4g). The parameters $\alpha_i^{\{\mathrm{p,lse,bm}\}}$ parameterize the shape along the NMPC prediction index i and yield the *smoothest* over-approximation for $i = N$ and the tightest for $i = 0$.

Corollary III.1. *With any of the three constraint homotopies, the resulting NMPC formulation satisfies recursive feasibility if the homotopy parameters α are chosen as a non-increasing sequence, i.e., $\alpha_i \geq \alpha_{i'}$ for $i \leq i'$.*

Proof. This follows directly from the tightening property together with the terminal constraint $v_N = 0$. □

E. Implementation using RTI Scheme

In the RTI scheme for NMPC, only one QP is solved per time step, where the QP is constructed by linearizing around the shifted solution guess from the previous time step. Due to the high sampling rates of the controller and relatively slow parameter changes in the problem, the RTI solution *tracks* the optimum [1] *over time*.

The presented algorithm is particularly suited for RTI since the shape parameters α along the horizon remain constant throughout iterations. A contrary approach would be to solve several QPs in one time step with an increasing shape parameter α in each iteration, i.e., a homotopy in α, but equal for the whole horizon. The latter requires multiple QP iterations per time step and is therefore computationally more expensive than the RTI scheme. Additionally, the initial guess at the beginning of each next time step could be infeasible due to the smoothed constraints.

The homogeneity property of the *ScaledNorm* formulation is particularly beneficial for RTI since even if the SQP method did not fully converge, the linearization is exact. Thus, no over-approximation error due to the linearizations is made.

IV. Simulation Experiments

Within closed-loop NMPC simulations using a single-track vehicle model, it is shown, how the progressive smoothing of obstacle shapes outperforms the ellipsoidal formulation of [7], the approach of [10], referred to as ReLU^2, covering circles [15], [16] and higher-order ellipsoids fixed along the whole horizon [9].

As an illustrative example, an evasion of two static obstacles is simulated for the *ScaledNorm* and the 2-norm, where the planned trajectories and the actually driven trajectories are compared, cf., Fig. 5. Furthermore, two randomized scenarios are simulated while evaluating key performance indicators.

A. Setup

The experiments involve two different simulation setups, where each experiment highlights a representative key performance indicator. Both experiments involve a randomized road, a simulated ego vehicle and one slower preceding SV, formulated as single-track models as in [7]. The simulated states are $\hat{x}_i$ at the simulation time $t = it_{\mathrm{d}}$. One single simulation is executed for $t_{\mathrm{sim}} = 15$ seconds, corresponding to $N_{\mathrm{sim}} = \frac{t_{\mathrm{sim}}}{t_{\mathrm{d}}}$ simulation steps, which generously allows overtaking. Parameters for both vehicles are taken from the `devbot 2.0` specification, which can be found in [20], and which correspond to a full-sized race car that was used in the real-world competition `Roborace` [27]. For the SV, the

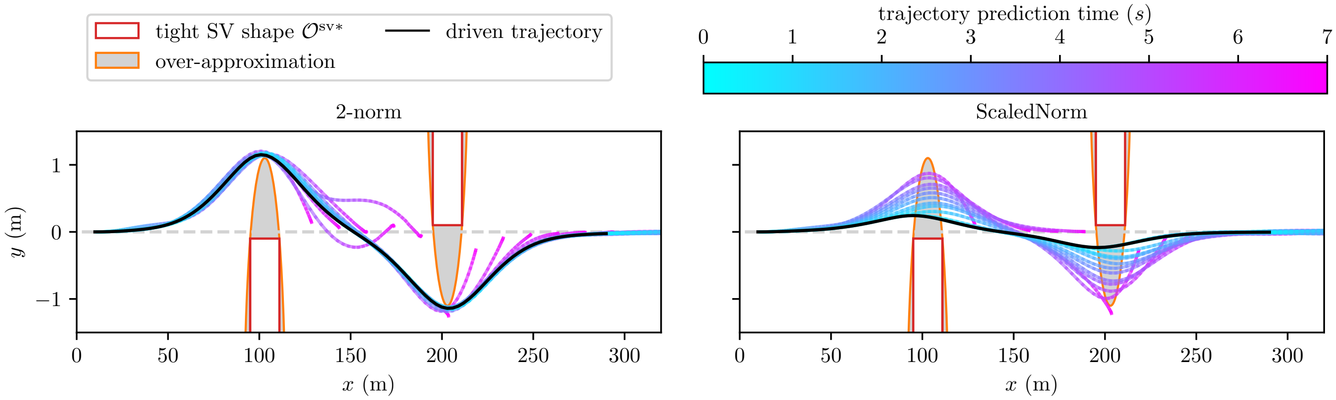

Fig. 5. Comparison of two evasion maneuvers for the 2-norm and the *ScaledNorm* formulation for a closed-loop simulation of $12s$. The 2-norm formulation leads to the ego vehicle evading the two static obstacles conservatively due to the inflated shape of the SV. On the other hand, using the *ScaledNorm* formulation, the smooth transition of conservatively evading planned trajectories towards a tightly driven trajectory (black) is visible.

<table>
<tr><th rowspan="2">Parameter</th><th colspan="2">Values</th></tr>
<tr><th>Experiment 1</th><th>Experiment 2</th></tr>
<tr><td>curvature</td><td colspan="2">$[0.01, 0.06]\frac{1}{\text{m}}$</td></tr>
<tr><td>road width</td><td colspan="2">10m</td></tr>
<tr><td>SV set velocity</td><td colspan="2">$[0, 5]\frac{\text{m}}{\text{s}}$</td></tr>
<tr><td>SV width</td><td colspan="2">$[1.5, 4]$m</td></tr>
<tr><td>SV length</td><td>$[4, 14]$m</td><td>$[2, 10]$m</td></tr>
<tr><td>SV start pos.</td><td colspan="2">$[50, 120]$m</td></tr>
<tr><td>ego set velocity</td><td colspan="2">$[7, 15]\frac{\text{m}}{\text{s}}$</td></tr>
<tr><td>ego weight w_n</td><td>5</td><td>50</td></tr>
<tr><td>ego start pos.</td><td colspan="2">$[0, 10]$m</td></tr>
</table>

TABLE II

PARAMETERS USED FOR SIMULATION. RANDOMIZED PARAMETERS ARE UNIFORMLY SAMPLED FROM THE GIVEN INTERVAL.

chassis width and length, as well as the maximum speed were randomized to capture different shapes. In the following, the individual simulation setups are described and associated parameters are shown in Tab. II.

Experiment 1 - Lateral Distance: The first experiment evaluates the maximum lateral distance

$$\Delta n_{\max} = \max_{i \in \mathbb{J}} \left| \hat{n}_i - n_i^{\text{SV}} - \frac{w}{2} \right|$$

and minimum lateral distance

$$\Delta n_{\min} = \min_{i \in \mathbb{J}} \left| \hat{n}_i - n_i^{\text{SV}} - \frac{w}{2} \right|,$$

where

$$\mathbb{J} = \left\{ i \in \mathbb{I}(N_{\text{sim}}) \middle| s_i^{\text{SV}} - \frac{l}{2} \leq \hat{s}_i \leq s_i^{\text{SV}} + \frac{l}{2} \right\}$$

while overtaking, cf. Fig. 7. It reveals that the actual driven trajectory is influenced by the over-approximations and verifies whether the constraint was violated.

Experiment 2 - Center Line Tracking: In many real-world applications, the driving cost is partly specified by tracking a certain reference line, which involves a higher cost to avoid cutting corners. If this cost is high or if the slower preceding SV has a larger width, a local minimum of the optimization problem (4) may be created behind the SV. Non-smooth SV shape representations tend to promote this local minimum, which is evaluated in the second experiment, by placing the SV in front of the ego vehicle. The performance measure Δs is the difference between the maximum reachable final position and the actual final position, written as

$$\Delta s = \hat{s}_0 + \tilde{v} t_{\text{f}} - \hat{s}_{N_{\text{sim}}-1},$$

with the positions $\hat{s}_i$ and the set velocity $\tilde{v}$ at the final simulation time t_{sim}.

Nonlinear Model Predictive Controller: The NMPC is formulated using the NLP (4) with the different SV approximations according to (5) and model parameters according to the `devbot`, cf. [20], [27].

The shape parameters $\alpha_i^{\{\cdot\}}$ at index i are determined implicitly, by defining the width and the height $\tilde{d}_i$ of the square obstacle shape at the axes of the auxiliary coordinates ξ, and implicitly solving the equation

$$o^{\{\cdot\}} \left([0,\ \tilde{d}_i]^\top, \alpha_i^{\{\cdot\}} \right) = 1$$

offline. The width $\tilde{d}$ can vary between $\tilde{d} = 1$, which would correspond to the exact rectangle and $\tilde{d} = \sqrt{2}$, corresponding to the circle or the 2-norm. In the experiments, we linearly change the over-approximated width from $\tilde{d}_0 = 1.005$ to $\tilde{d}_N = \sqrt{2}$ which implicitly defines the shape parameters $\alpha_i^{\{\cdot\}}$ for all steps i.

Fig. 1 shows the related shapes for indexes $i \in \{0, \frac{N}{2}, N\}$. By defining the shape based on the width, the progressive smoothing formulations are nearly equal in terms of their over-approximated area and allow for fair comparisons between the different approaches.

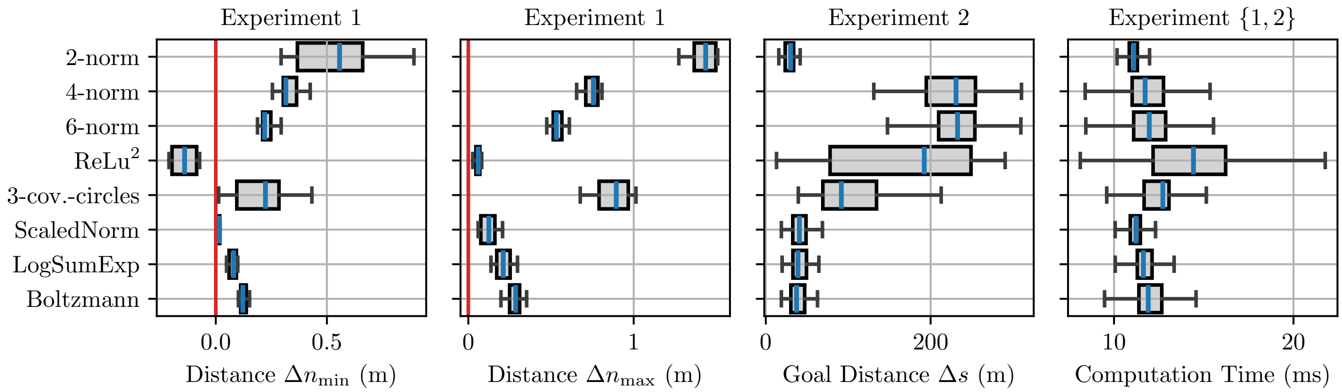

Fig. 6. Box-plot performance evaluation of the proposed approaches in different randomized closed-loop experiments. In *Experiment 1*, the maximum and minimum lateral distance $\Delta n_{\max}$ and $\Delta n_{\min}$ to an SV while overtaking is evaluated. A negative distance indicates an unsafe constraint violation (red line) as observed with the ReLU^2 formulation. In *Experiment 2*, the goal distance Δs, i.e., the difference of the maximum reachable position to the actual position, after overtaking at the final simulation time t_{sim} is evaluated. The computation time was evaluated for all experiments.

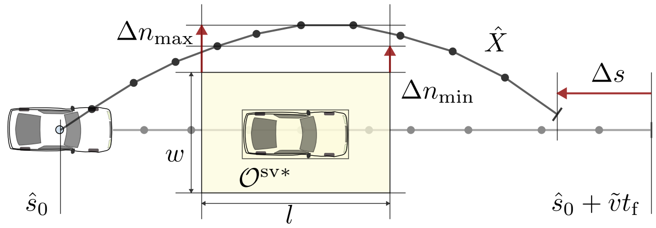

Fig. 7. Sketch of the evaluated performance measures of the simulated trajectory $\hat{X}$, including the minimal and maximal overtaking distance $\Delta n_{\min}$ and $\Delta n_{\max}$, respectively, and the distance Δs to the maximum position that could be reached without SVs.

Implementation details: To solve the NMPC problem (4), the solver `acados` [28], together with the QP solver `HPIPM` [29] is used. We use RTI, without condensing, an explicit RK4 integrator and a Gauss-Newton Hessian approximation. For the prediction, $N = 70$ shooting nodes are used with a discretization time of $t_{\mathrm{d}} = 0.1$ seconds which corresponds to a prediction horizon of 7 seconds.

B. Evaluation

In Fig. 5, actual driven and planned trajectories of an overtaking maneuver are shown in the Cartesian coordinates. It can be seen in the left plot that the ellipsoidal formulation leads to conservative behavior, in which the ego vehicle performs strong lateral swaying maneuvers to avoid any potential collision with the SVs.

In Fig. 6, the key performance measures of the experiments are shown. As already indicated by Fig. 5, the maximum lateral distance $\Delta n_{\max}$ is largest for the ellipsoidal formulation. Higher order ellipsoids, such as the 4-norm and the 6-norm, yield superior results for the maximum lateral distance, similar to the proposed progressive smoothing and ReLU^2 formulations.

When evaluating the minimum distance $\Delta n_{\min}$ while overtaking, the ReLU^2 formulation reveals a disadvantageous property, i.e., even though the obstacle slack variables are chosen as exact penalties (L1 penalization) for all formulations with equal weights, the constraints are violated. This issue was mentioned in [10] and circumvented by an increased over-approximation. All other methods respect the constraints exactly and are therefore considered safe.

With an increased center line tracking cost, the constant higher order ellipsoids, covering circles and the ReLU^2 formulation repeatedly get stuck in the local minima behind the preceding SV, limiting its performance and getting blocked behind. This problem is the main reason why other works suggest not using constant higher-order norms and rather using the 2-norm [7], [21]. For any overtaking objectives, this problem can be limiting. The simulation results empirically show that the proposed approaches are less likely to get stuck in a local minimum, and therefore lead to an improved performance for this particular case study.

In the final plot of Fig. 6, the computation times among all experiments are shown and verify that the computation time is similar for each of the considered NMPC formulations, despite an average increase of the median computation time by 27.2% and the maximum computation time by 60.9% using the ReLU^2 formulation compared to the *ScaledNorm*.

The *ScaledNorm* formulation has a good performance in all evaluations, taking into account the constraint violation of the ReLU^2 formulation. The reason for the *ScaledNorm* performing better than *LogSumExp* and *Boltzmann* may be the exact constraint linearization related to the norm function. Despite the good performance of also the *Boltzmann* formulation, it can not be guaranteed that the linearized constraint safely over-approximates the obstacle shape [7] due to its non-convex shape.

V. Conclusions

A novel progressive smoothing scheme was presented for obstacle avoidance in NMPC. The presented *ScaledNorm* approach, as well as the alternative formulations *Boltzmann* and *LogSumExp* outperform the benchmarks, including fixed higher-order ellipsoids [9], covering circles [15], [16] and the formulation used in [10]. The performance achieved by the *ScaledNorm* is superior to all others in these particular experiments, which is likely due to the advantageous linearizations of the norm function. The alternative *Boltzmann* formulation has the drawback of non-convexity. Moreover, the *ScaledNorm* formulation has desirable theoretical properties, such as convexity, tightening, homogeneity, exact slack penalty and over-approximation.

ACKNOWLEDGMENT

Rudolf Reiter, Katrin Baumgärtner and Moritz Diehl were supported by EU via ELO-X 953348, by DFG via Research Unit FOR 2401, project 424107692 and 525018088 and by BMWK via 03EI4057A and 03EN3054B.

REFERENCES

[1] M. Diehl, H. G. Bock, and J. P. Schlöder, "A real-time iteration scheme for nonlinear optimization in optimal feedback control," *SIAM Journal on Control and Optimization*, vol. 43, no. 5, pp. 1714–1736, 2005.

[2] U. Rosolia and F. Borrelli, "Learning model predictive control for iterative tasks. a data-driven control framework," *IEEE Transactions on Automatic Control*, vol. 63, no. 7, pp. 1883–1896, 2018.

[3] D. Kloeser, T. Schoels, T. Sartor, A. Zanelli, G. Prison, and M. Diehl, "NMPC for racing using a singularity-free path-parametric model with obstacle avoidance," *IFAC-PapersOnLine*, vol. 53, no. 2, pp. 14 324–14 329, 2020, 21st IFAC World Congress.

[4] J. L. Vázquez, M. Brühlmeier, A. Liniger, A. Rupenyan, and J. Lygeros, "Optimization-based hierarchical motion planning for autonomous racing," in *IEEE/RSJ International Conference on Intelligent Robots and Systems (IROS)*, 2020, pp. 2397–2403.

[5] X. Xing, B. Zhao, C. Han, D. Ren, and H. Xia, "Vehicle motion planning with joint cartesian-frenet MPC," *IEEE Robotics and Automation Letters*, vol. 7, no. 4, pp. 10 738–10 745, 2022.

[6] A. Raji, A. Liniger, A. Giove, A. Toschi, N. Musiu, D. Morra, M. Verucchi, D. Caporale, and M. Bertogna, "Motion planning and control for multi vehicle autonomous racing at high speeds," in *IEEE 25th International Conference on Intelligent Transportation Systems (ITSC)*, 2022, pp. 2775–2782.

[7] R. Reiter, A. Nurkanović, J. Frey, and M. Diehl, "Frenet-cartesian model representations for automotive obstacle avoidance within nonlinear MPC," *European Journal of Control*, p. 100847, 2023.

[8] K. Bergman and D. Axehill, "Combining homotopy methods and numerical optimal control to solve motion planning problems," in *IEEE Intelligent Vehicles Symposium (IV)*, 2018, pp. 347–354.

[9] A. Schimpe and F. Diermeyer, "Steer with me: A predictive, potential field-based control approach for semi-autonomous, teleoperated road vehicles," in *IEEE 23rd International Conference on Intelligent Transportation Systems (ITSC)*, 2020, pp. 1–6.

[10] A. Sathya, P. Sopasakis, R. Van Parys, A. Themelis, G. Pipeleers, and P. Patrinos, "Embedded nonlinear model predictive control for obstacle avoidance using PANOC," in *European Control Conference (ECC)*, 2018, pp. 1523–1528.

[11] M. Geisert and N. Mansard, "Trajectory generation for quadrotor based systems using numerical optimal control," in *IEEE International Conference on Robotics and Automation (ICRA)*, 2016, pp. 2958–2964.

[12] S. H. Nair, E. H. Tseng, and F. Borrelli, "Collision avoidance for dynamic obstacles with uncertain predictions using model predictive control," in *IEEE 61st Conference on Decision and Control (CDC)*, 2022, pp. 5267–5272.

[13] T. Schoels, P. Rutquist, L. Palmieri, A. Zanelli, K. O. Arras, and M. Diehl, "Ciao∗: MPC-based safe motion planning in predictable dynamic environments," *IFAC-PapersOnLine*, vol. 53, no. 2, pp. 6555–6562, 2020, 21st IFAC World Congress.

[14] Y. Oh, M. H. Lee, and J. Moon, "Infinity-norm-based worst-case collision avoidance control for quadrotors," *IEEE Access*, vol. 9, pp. 101 052–101 064, 2021.

[15] J. Ziegler, P. Bender, T. Dang, and C. Stiller, "Trajectory planning for bertha - a local, continuous method," in *IEEE Intelligent Vehicles Symposium, Proceedings*, 06 2014, pp. 450–457.

[16] J. Wang, Y. Yan, K. Zhang, Y. Chen, C. Mingcong, and G. Yin, "Path planning on large curvature roads using driver-vehicle-road system based on the kinematic vehicle model," *IEEE Transactions on Vehicular Technology*, vol. PP, pp. 1–1, 11 2021.

[17] S. Brossette and P.-B. Wieber, "Collision avoidance based on separating planes for feet trajectory generation," 11 2017, pp. 509–514.

[18] A. Zanelli, "Inexact methods for nonlinear model predictive control: stability, applications, and software," Ph.D. dissertation, University of Freiburg, 2021.

[19] K. Baumgärtner, A. Zanelli, and M. Diehl, "Stability analysis of nonlinear model predictive control with progressive tightening of stage costs and constraints," *IEEE Control Systems Letters*, vol. 7, pp. 3018–3023, 2023.

[20] R. Reiter, M. Kirchengast, D. Watzenig, and M. Diehl, "Mixed-integer optimization-based planning for autonomous racing with obstacles and rewards," *IFAC-PapersOnLine*, vol. 54, no. 6, pp. 99–106, 2021, 7th IFAC Conference on Nonlinear Model Predictive Control NMPC 2021.

[21] R. Reiter, J. Hoffmann, J. Boedecker, and M. Diehl, "A hierarchical approach for strategic motion planning in autonomous racing," in *European Control Conference (ECC)*, 2023, pp. 1–8.

[22] M. Werling, J. Ziegler, S. Kammel, and S. Thrun, "Optimal trajectory generation for dynamic street scenarios in a frenet frame," in *Proceedings - IEEE International Conference on Robotics and Automation*, 06 2010, pp. 987 – 993.

[23] M. Schuurmans, A. Katriniok, C. Meissen, H. E. Tseng, and P. Patrinos, "Safe, learning-based MPC for highway driving under lane-change uncertainty: A distributionally robust approach," *Artificial Intelligence*, vol. 320, p. 103920, 2023.

[24] H. Bock and K. Plitt, "A multiple shooting algorithm for direct solution of optimal control problems*," *IFAC Proceedings Volumes*, vol. 17, no. 2, pp. 1603–1608, 1984, 9th IFAC World Congress: A Bridge Between Control Science and Technology, Budapest, Hungary, 2-6 July 1984.

[25] J. B. Rawlings, D. Q. Mayne, and M. M. Diehl, *Model Predictive Control: Theory, Computation, and Design*, 2nd ed. Nob Hill, 2017.

[26] Q. Tran Dinh, S. Gumussoy, W. Michiels, and M. Diehl, "Combining convex–concave decompositions and linearization approaches for solving bmis, with application to static output feedback," *IEEE Transactions on Automatic Control*, vol. 57, no. 6, pp. 1377–1390, 2012.

[27] Ltd. Roborace. 2019. Roborace. [Online]. Available: https://roborace.com/

[28] R. Verschueren, G. Frison, D. Kouzoupis, J. Frey, N. van Duijkeren, A. Zanelli, B. Novoselnik, T. Albin, R. Quirynen, and M. Diehl, "acados – a modular open-source framework for fast embedded optimal control," *Mathematical Programming Computation*, Oct 2021.

[29] G. Frison and M. Diehl, "HPIPM: a high-performance quadratic programming framework for model predictive control," *IFAC-PapersOnLine*, vol. 53, no. 2, pp. 6563–6569, 2020, 21st IFAC World Congress.